RELAX-BASED ESTIMATION OF VOIGT LINESHAPES

Stefan Ingi Adalbjörnsson and Andreas Jakobsson

Dept. of Mathematical Statistics, Lund University, Sweden
sia@maths.lth.se, aj@maths.lth.se

ABSTRACT

Most spectroscopic signals are well described as having either a Lorentzian or Gaussian lineshape, and the recent literature contains a variety of estimation approaches for such models. However, several experimental works indicate that such signals can be better described as having the more general Voigt lineshape, formed as the combination of the two. Due to the inherent complexity of this model, there exist few techniques to form estimates of the parameters of the Voigt model, with a numerical search of the multidimensional nonlinear least squares (LS) cost function being the typical solution. In this paper, we propose a parametric relax-based estimator that estimates the lineshape parameters recursively, one spectral line at a time. Numerical simulations using both simulated and real measurement data illustrate the performance gain of the proposed methods.

1. INTRODUCTION

Currently, most spectroscopic signals are described as either having a Lorentzian or possibly a Gaussian lineshape, and much work has been done on finding methods for efficiently estimating the parameters describing these models (see, e.g., [1–5]). These models are popular and generally work well, although several experimental studies indicate that many forms of spectroscopic signals are better described as having a Voigt lineshape. The structure and/or form of the lineshape plays an important role in several applications, for instance, in the detection of counterfeit medicines, and there is a strong need to develop reliable techniques for improving the estimates of the parameters detailing the spectral lines. Regrettably, due to the complexity of the Voigt model, few efficient estimation techniques exist to date, with numerical search of the least squares (LS) cost function in either the time or frequency domain being the most typical solution [6–8]. Such techniques are generally computationally cumbersome and require an accurate initial value for the search spaces. In this paper, we propose a parametric relaxation-based technique for estimating the lineshape parameters from a (possibly) non-uniformly sampled free induction decay (FID) or, alternatively, a sequence of echo signals, resulting from, for example, a pulse spin-locking (PSL) excitation sequence. Such a sequence of echoes are here termed an echo train (ET) sequence (see, e.g., [9, 10]). In [11], and later in the extended version presented in [12] (see also [13]), it has been shown that relaxation-based methods offer excellent estimation performance even in the presence of colored noise. By alternatively estimating one component at a time, this form of approaches can often also be implemented quite efficiently. In the here presented extension of the methods in [11,12], we exploit both the detailed structure of the signal as well as initial frequency estimates, formed using either the regular periodogram, or IAA [14, 15] for the case of non-uniformly sampled data, to restrict the dimensionality of the search space. Numerical studies indicate that the presented method offers parameter estimates with close to optimal performance, even though the procedure assumes that the problem decouples, reducing the dimensionality of the performed search substantially. Evaluating the method on real measurements of the explosive TNT indicates that the model improves parameter estimates for this substance somewhat.

2. DATA MODEL

Spectroscopic signals are most commonly measured as either FIDs or ET sequences. In the following, we shall examine both these forms of signals, extending the models to also include a Voigt parameter. Incorporating this extension, the measured FID signal formed from d resonant lines can thus be modeled as [9]

$$y_{\text{fid}}(t) = \rho \sum_{k=1}^{d} \tilde{\kappa}_k e^{-\beta_k t - \gamma_k t^2 + i\omega_k(T)t} + w(t), \qquad (1)$$

where $t = t_0, \ldots, t_{N-1}$ is the FID sampling time, $w(t)$ is an additive colored noise and ρ denotes the common scaling due to the signal to noise ratio (SNR). We note that the underlying thermal (Johnson) noise at the RF antenna may often be well modeled as a white Gaussian noise (WGN) process. However, the noise is then typically colored by the receiver, making it more appropriately modeled as the output of an autoregressive (AR) filter driven by WGN [16]. Furthermore, the normalized (complex) amplitudes of the FID, here denoted $\tilde{\kappa}_k$ for the kth line, can be assumed to be fairly well known for a given experimental set-up, although these may vary in between setups and due to, e.g., the crystalline properties of the sample. The damping and Voigt constants, β_k and γ_k, for the kth line are often reasonably well known, but may vary significantly due to, e.g., sample impurities, and are therefore better to treat as unknown within some limited set. Finally, the frequencies, $\omega_k(T)$, typically depends on the (unknown) temperature of the examined sample, such that for a given temperature, T, the frequencies are known, typically following $\omega_k(T) = a_k + b_k T$, for some given constants a_k and b_k [16]. Echo trains on the other hand will contain further structure, and the noise-free mth echo of an echo train may be well modeled as [9]

$$y^m(t) = \rho \sum_{k=1}^{d} \kappa_k e^{-\eta_k m\mu} \zeta_k^t e^{-\beta_k|t-t_{sp}| - \gamma_k|t-t_{sp}|^2}, \qquad (2)$$

where $\zeta_k = e^{i\omega_k(T)-\eta_k}$ and $t = t_0, \ldots, t_{N-1}$ is the echo sampling time[1], measured with respect to the center of the re-

[1] For notational convenience, we will here use the same notation for the FID and the ET sampling times, although these are generally different.

 ISSN 2076-1465

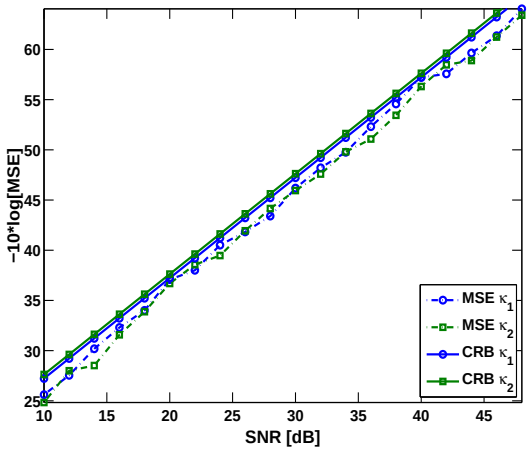

Figure 1: MSE error for the estimated amplitudes as compared to the corresponding CRB.

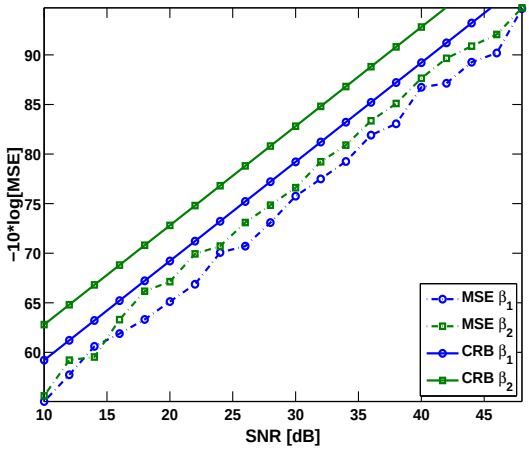

Figure 2: MSE error for the estimated β_1 and β_2 plotted as compared to the corresponding CRB.

focusing pulse, not necessarily being consecutive instances, but typically starting at $t_0 \neq 0$ to allow for the dead time between the pulse and the first measured sample (after the pulse). Here, t_{sp} and μ are known constants. It should be noted that the normalized (complex) amplitudes for the echo train, here denoted κ_k for the kth component, are different to $\tilde{\kappa}_k$, with the former being also dependent on t_{sp}.

3. THE VOIGT RELAX ALGORITHM

As the data sequences detailed by either (1) or (2) are often non-uniformly sampled due to the gaps resulting from the pulsing and the following dead time(s), initial estimates of the line frequencies should then be formed using a technique robust to such signals. Furthermore, given that spectroscopic sequences are often corrupted by (substantial) radio frequency interference (RFI) and other spurious signals, as well as being measured in the presence of colored noise, we recommend forming initial frequency estimates using either the periodogram, for regularly sampled data, or the non-parametric IAA algorithm [14, 15], for more arbitrary sampling patterns. Using either method, we form initial estimates of the unknown line frequencies, and then proceed to form the relax estimate over the parameters β_k, γ_k and η_k, if relevant, for these frequencies. Let $\mathbf{y}_{\tilde{N}}$ denote the (column) vector formed from the available measurement samples; for the FID measurements, obtained from, e.g., a stochastic NQR (sNQR) experiment [10], $\tilde{N} = N$, whereas for an ET measurement the total number of available samples is $\tilde{N} = NM$, where M denotes the number of available echoes (see, e.g., [9])). Moreover, let

$$\mathbf{y}_{\tilde{N}} = \rho \sum_{k=1}^{d} \alpha_k \mathbf{A}_{\theta,k}^{(i)} + \mathbf{e}_{\tilde{N}} \tag{3}$$

denote the vectorized model corresponding to either (1) or (2), where α_k denotes the assumed amplitudes $\tilde{\kappa}_k$ or κ_k, and θ contain the unknown parameters detailing the model, i.e.,

$$\begin{aligned} \theta^{(1)} &= \left[\begin{array}{cccc} T & \rho & \{\beta_k\}_{k=1}^{d} & \{\gamma_k\}_{k=1}^{d} \end{array} \right]^T \\ \theta^{(2)} &= \left[\begin{array}{ccccc} T & \rho & \{\beta_k\}_{k=1}^{d} & \{\gamma_k\}_{k=1}^{d} & \{\eta_k\}_{k=1}^{d} \end{array} \right]^T \end{aligned}$$

for (1) and (2), respectively. The (column) vector $\mathbf{A}_{\theta,k}^{(i)}$ is formed as the vectorized form from the kth spectral line from either (1) or (2) corresponding to $\mathbf{y}_{\tilde{N}}$, and $\mathbf{e}_{\tilde{N}}$ is formed similar to $\mathbf{y}_{\tilde{N}}$. Thus for (1) and (2), $\mathbf{A}_{\theta,k}^{(i)}$ is given by $\mathbf{A}_{\theta,k}^{1}$ in equation (4) and $\mathbf{A}_{\theta,k}^{2}$ in equation (6), respectively, listed at the top of the next page. The non-linear least squares (NLS) estimate of θ can be found as

$$\hat{\theta}_{NLS} = \arg\min_{\theta} \left\| \mathbf{y}_{\tilde{N}} - \rho \sum_{k=1}^{d} \alpha_k \mathbf{A}_{\theta,k}^{(i)} \right\|^2 \tag{6}$$

for $i = 1$ or 2, where $\|\cdot\|$ denotes the Euclidean norm. As is well known, the $\hat{\theta}_{NLS}$ estimate will only coincide with the maximum likelihood estimate when the additive noise $\mathbf{e}_{\tilde{N}}$ is a zero-mean white Gaussian process, although, under quite weak assumptions, the estimates will achieve the same asymptotical performance even for the colored noise case [17]. Reminiscent to [11, 12], we proceed to form the relax-based estimate of θ by minimizing the cost function in (6) in a recursive fashion, one component at a time. Let

$$\mathbf{y}_{\tilde{N},\ell} = \mathbf{y}_{\tilde{N}} - \rho \sum_{k=1,k\neq\ell}^{d} \alpha_k \mathbf{A}_{\theta,k}^{(i)} + \mathbf{e}_{\tilde{N}} \tag{7}$$

where

$$\theta_k = \left[\begin{array}{ccc} \beta_k & \gamma_k & \eta_k \end{array} \right]^T, \tag{8}$$

for $k = 1, k \neq \ell$, are assumed to be known from prior estimation steps. Then, the NLS estimate of θ_ℓ can be found as

$$\hat{\theta}_\ell = \arg\min_{\theta} \left\| \mathbf{y}_{\tilde{N},\ell} - \rho\alpha_\ell \mathbf{A}_{\theta,\ell}^{(i)} \right\|^2 \tag{9}$$

$$= \arg\max_{\theta} \left\{ \left| \mathbf{A}_{\theta,\ell}^{(i)*} \mathbf{y}_{\tilde{N},\ell} \right|^2 / (\mathbf{A}_{\theta,\ell}^{(i)*} \mathbf{A}_{\theta,\ell}^{(i)}) \right\} \tag{10}$$

where $(\cdot)^*$ denotes the conjugate transpose. It is worth noting that the maximization in (10) can be efficiently performed using numerical optimization techniques, such as, for instance, a Levenberg-Marquardt or a Gauss-Newton method (see, e.g., [18, 19]). The relaxation-based estimate of θ is

$$A^1_{\theta,k} = \left[\begin{array}{ccc} e^{-\beta_k t_1 - \gamma_k t_1^2 + i\omega_k(T)t_1} & \dots & e^{-\beta_k t_1 - \gamma_k t_1^2 + i\omega_k t_N} \end{array} \right]^T \quad (4)$$

$$A^2_{\theta,k} = [(\tilde{f}^1_{\theta,k}), \dots, (\tilde{f}^M_{\theta,k})]^T \quad (5)$$

$$\tilde{f}^m_{\theta,k} = \left[\begin{array}{ccc} e^{-\eta_k m\mu}\zeta_k^{t_1} e^{-\beta_k|t_1-t_{sp}|-\gamma_k|t_1-t_{sp}|^2} & \dots & e^{-\eta_k m\mu}\zeta_k^{t_N} e^{-\beta_k|t_N-t_{sp}|-\gamma_k|t_N-t_{sp}|^2} \end{array} \right]$$

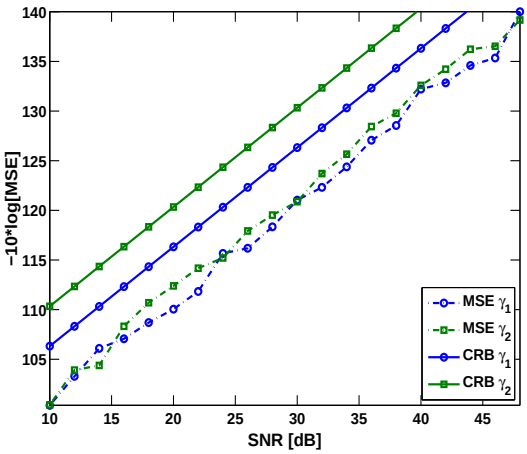

Figure 3: MSE error for the estimated γ_1 and γ_2 as compared to the corresponding CRB.

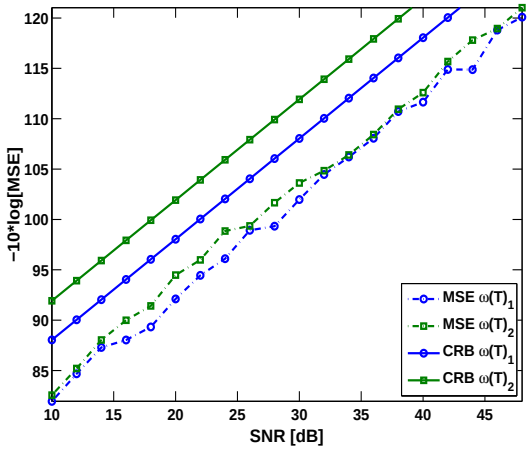

Figure 4: MSE error for the estimated frequencies as compared to the corresponding CRB.

thus formed as follows (see also [11, 12] for further details on the recursive steps):

Step 0. Form initial estimates of the unknown frequencies using the periodogram or the IAA algorithm in case of non-uniformly sampled data.
Step 1. Assume $d = 1$, and compute $\hat{\theta}_1$ from $\mathbf{y}_{\tilde{N}}$ using (10).
Step 2. Assume $d = 2$. Compute $\mathbf{y}_{\tilde{N},2}$ with (7) using $\hat{\theta}_1$, and then estimate $\hat{\theta}_2$ using (10) with $\mathbf{y}_{\tilde{N},2}$. Then, form $\mathbf{y}_{\tilde{N},1}$ using $\hat{\theta}_2$ and reestimate $\hat{\theta}_1$. Substeps 1 and 2 are then iterated until practical convergence is achieved.
Step 3. Proceed by growing the assumed d to $d = 3, 4, \dots$, until the desired number of spectral lines. For each value of d, $\hat{\theta}_k$, for $k = 1, \dots, d$, is estimated recursively using the approach in steps 1 and 2, with each step extended to recursively estimate all the d lines.

The above mentioned practical convergence is typically set as when the relative change of the cost function between two consecutive iteration is below some predetermined cut-off point, for instance, when the change is less than $\varepsilon = 10^{-8}$. We note that as a minimization is performed at each step, the algorithm is bound to converge to a local minimum under mild conditions (although, the achieved minimum might, of course, possibly not be the global one). It should also be stressed that due to the recursive nature of the algorithm, the computational complexity is proportional to d^2 for large d, and can thus be computationally demanding for signals containing a large number of spectral lines. For our considered applications, d is typically small, with generally $d < 5$.

4. NUMERICAL EXAMPLES

In this section, we examine the performance of the proposed estimator using both simulated and real measurement data. Initially, we examine simulated FID data mimicking a generic sNQR measurement of a pharmaceutical substance of interest, assuming $d = 2$, with $N = 200$, $\omega(T) = \{0.3, 0.45\}$, $\beta = \{2.056, 4.567\} \times 10^{-4}$, $\gamma = \{2.008, 3.002\} \times 10^{-5}$, and $\tilde{\kappa} = \{0.75, 1\}$.The measurements are formed using (1), where $e(t)$ is modeled as a zero-mean circularly symmetric white Gaussian noise process with variance σ_w^2. Figures 1-4 show the mean-squared error (MSE) as compared to the corresponding Cramér-Rao lower bound (CRB), as derived in the Appendix. These simulations were obtained using 100 Monte Carlo simulations. As can be seen from the figures, the relax estimator achieves performance being close to efficient. However, it should also be noted that given the parameter values of typical samples of interest, the estimation variance might well be on the order of the actual value of interest, or indeed significantly larger than these values. Figures 5 and 6 illustrate this problem by plotting the root relative CRB (RRCRB), defined as 100 times the square root of the CRB divided by the true parameter value, for the β_1 parameter as a function of $\gamma_1 = -\{4.5, 19.7, 34.8\} \times 10^{-5}$, and for γ_1 for $\beta_1 = -\{4.95, 2.47, 0.0505\} \times 10^{-4}$, respectively. As seen from the figure, the variance of the β estimate is strongly affected by the size of the γ parameter, whereas the variance of the γ estimate is seemingly unaffected by changes in the damping parameter. However, from Figure 5, it is clear that the more detailed Voigt modeling will not offer any improvement of the β estimates for substances with a combination of too low β and γ values, and it is recommended that the RRCRB is evaluated for any

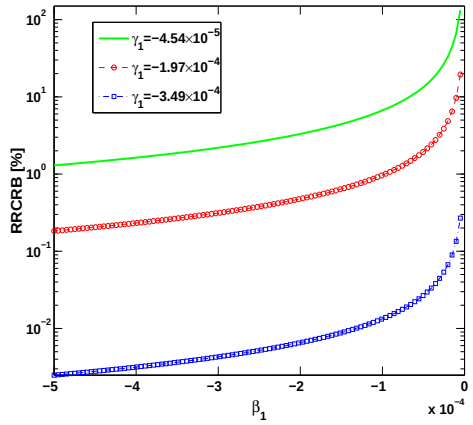

Figure 5: The RRCRB of the β_1 parameter in the numerical example, where β_1 is varied for three different values of γ_1.

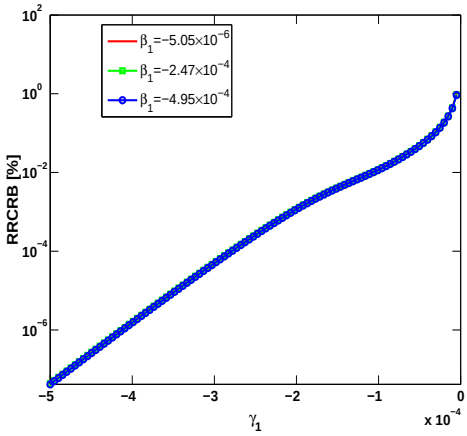

Figure 6: The RRCRB of the γ_1 parameter in the numerical example, where γ_1 is varied for three different values of β_1.

Line no.	1	2	3	4
$\omega_k(T)/2\pi$	0.201	0.074	0.022	-0.146
$\beta_k \times 10^{-3}$	0.00	11.52	0.68	3.38
$\gamma_k \times 10^{-3}$	0.23	0.00	0.00	0.00
$\eta_k \times 10^{-3}$	0.18	0.26	0.22	0.22
$\lvert\kappa_k\rvert$	0.16	1.00	0.54	0.61

Table 1: Estimated parameters detailing the four dominant TNT lines in the dataset examined in [16].

examined substance to determine the SNR and data length required to make the model useful. We proceed to examine real ET measurements from the explosive TNT. Using the NQR data examined in [16], with $N = 256$, $M = 31$, we apply the relax algorithm now instead formed using (6). The resulting parameter estimates are given in Table 1, where it can be seen that only one of the four spectral lines have a noticeable value for γ. Interestingly, the β-value for this line is negligible, indicating that this spectral line has a Gaussian, and not a Lorentzian or Voigt, lineshape. The found values decrease the sum of the squared residuals with 0.34% compared with the model used in [16], indicating that, as can be expected from the values in Table 1, the more detailed model allow for only a minor improvement of the signal model for TNT. Table 2 presents the RRCRB for the estimated parameters, showing that, for instance, the standard deviation of γ_1 is about 9% of the estimated parameter value, indicating that this parameter can be fairly well determined. On the other hand, one may note that β_3 seems not to be possible to estimate accurately, as can also be expected from the small value of this parameter.

5. ACKNOWLEDGEMENTS

The authors would like to thank the authors of [20] for providing us with their manuscript, as well as Dr. M. D. Rowe and Prof. J. A. S. Smith for providing the TNT measurement data. This work was supported in parts by the Swedish Research Council, Carl Tryggers Foundation, the Swedish Foundation for International Cooperation in Research and Higher Education (STINT), and the US National Science Foundation under Grant No. ECCS-0729727.

Line no.	1	2	3	4
β_k	–	4.14	68.7	14.3
γ_k	9.21	–	–	–
η_k	5.26	0.86	0.92	0.95

Table 2: The RRCRB for the estimated parameters detailing the four dominant TNT lines.

A. THE CRB FOR THE VOIGT MODELS

The CRB for the Voigt model in (1) omitting the temperature dependencies of the line frequencies was presented in [20]. Here, we extend on this derivation to incorporate also the temperature dependencies, as well as derive the CRB for the ET model in (2). For $t = t_0, \ldots, t_{N-1}$, $m = 0, \ldots, M-1$, let

$$\lambda_k(t) = e^{-\beta_k t - \gamma_k t^2 + i\omega_k(T)t} \quad (11)$$

$$\xi_k^m(t) = e^{-\eta_k m\mu}\zeta_k^t e^{-\beta_k|t-t_{sp}|-\gamma_k|t-t_{sp}|^2} \quad (12)$$

Using the same notation as in [20, 21], one thus obtain the CRB as

$$\mathbf{V}_\theta = \sigma^2\left(2Re\left[\frac{\partial \mathbf{x}_{\tilde{N}}}{\partial\theta}\left(\frac{\partial \mathbf{x}_{\tilde{N}}}{\partial\theta}\right)^H\right]\right)^{-1}, \quad (13)$$

where

$$\mathbf{x}_{\tilde{N}} = \rho\bar{\mathbf{x}}_{\tilde{N}} = \rho\sum_{k=1}^{d}\alpha_k\mathbf{A}_{\theta,k}^{(i)}, \quad (14)$$

which leads to (15) and (16), as given at the top of the next page, for (1) and (2), respectively.

REFERENCES

[1] J. Higinbotham and I. Marshall, "NMR Lineshapes and Lineshape Fitting Procedures," *Annu. Rep. NMR Spectrosc.*, vol. 43, pp. 59–120, 2001.

[2] L. Vanhamme, T. Sundin, P. V. Hecke, and S. V. Huffel, "MR spectroscopy quantitation: a review of time-domain methods," *NMR in Biomedicine*, vol. 14, no. 4, pp. 233 – 246, 2001.

$$\frac{\partial \mathbf{x}_{\tilde{N}}}{\partial \tilde{\theta}^{(1)}} = \left[j\rho \sum_{k=1}^{d} b_k \tilde{\kappa}_k f_{\theta,k},\ \bar{\mathbf{x}}_{\tilde{N}},\ -t f_{\theta,1},\ \ldots,\ -t f_{\theta,d},\ -t^2 f_{\theta,1},\ \ldots,\ -t^2 f_{\theta,d} \right] \tag{15}$$

$$\frac{\partial \mathbf{x}_{\tilde{N}}}{\partial \tilde{\theta}^{(2)}} = \Big[j\rho \sum_{k=1}^{d} b_k \tilde{\kappa}_k \hat{f}_{\theta,1},\ \bar{\mathbf{x}}_{\tilde{N}},\ -|t-t_{sp}|\hat{f}_{\theta,1},\ \ldots\ ,\ -|t-t_{sp}|\hat{f}_{\theta,d},\ -|t-t_{sp}|^2 \hat{f}_{\theta,1} \\ ,\ \ldots\ ,\ -|t-t_{sp}|^2 \hat{f}_{\theta,d},\ -(m\mu+t)\hat{f}_{\theta,1},\ldots,\ -(m\mu+t)\hat{f}_{\theta,d} \Big] \tag{16}$$

[3] S. Mierisova and M. Ala-Korpela, "MR spectroscopy quantitation: a review of frequency domain methods," *NMR in Biomedicine*, vol. 14, no. 4, pp. 247 – 259, 2001.

[4] J. B. Poullet, D. M. Sima, and S. van Huffel, "MRS signal quantification: a review of time- and frequency-domain methods," *Journal of magnetic resonance*, vol. 195, pp. 134–144, 2008.

[5] E. Gudmundson, P. Stoica, J. Li, A. Jakobsson, M. D. Rowe, J. A. S. Smith, and J. Ling, "Spectral estimation of irregularly sampled exponentially decaying signals with applications to RF spectroscopy," *Journal of Magnetic Resonance*, vol. 203, pp. 167–176, 2010.

[6] S. D. Bruce, J. Higinbotham, I. Marshall, and P. H. Beswick, "An Analytical Derivation of a Popular Approximation of the Voigt Function for Quantification of NMR Spectra," *Journal of Magnetic Resonance*, vol. 142, no. 1, pp. 57 – 63, 2000.

[7] I. Marshall, J. Higinbotham, S. Bruce, and A. Freise, "Use of Voigt lineshape for quantification of in vivo 1H spectra," *Magnetic Resonance in Medicine*, vol. 37, pp. 651 – 657, 2005.

[8] H. Ratiney, A. Bucur, M. Sdika, O. Beuf, F. Pilleul, and S. Cavassila, "Effective Voigt model estimation using multiple random starting values and parameter bounds settings for in vivo hepatic 1H magnetic resonance spectroscopic data," in *5th IEEE International Symposium on Biomedical Imaging*, May 2008, pp. 1529–1532.

[9] S. D. Somasundaram, A. Jakobsson, J. A. S. Smith, and K. Althoefer, "Exploiting Spin Echo Decay in the Detection of Nuclear Quadrupole Resonance Signals," *IEEE Trans. Geoscience and Remote Sensing*, vol. 45, no. 4, pp. 925–933, April 2007.

[10] S. D. Somasundaram, A. Jakobsson, M. D. Rowe, J. A. S. Smith, N. R. Butt, and K. Althoefer, "Robust Detection of Stochastic Nuclear Quadrupole Resonance Signals," *IEEE Transactions on Signal Processing*, vol. 56, no. 9, pp. 4221–4229, Sept. 2008.

[11] J. Li and P. Stoica, "Efficient Mixed-Spectrum Estimation with Applications to Target Feature Extraction," *IEEE Trans. Signal Processing*, vol. 44, no. 2, pp. 281–295, February 1996.

[12] Z.-S. Liu, J. Li, and P. Stoica, "Relax-based estimation of damped sinusoidal signal parameters," *Signal Processing*, vol. 62, pp. 311–321, 1997.

[13] Z.-S. Liu and J. Li, "Implementation of the RELAX Algorithm," *IEEE Trans. Aero. and Elec. Syst.*, vol. 34, no. 2, pp. 657–664, April 1998.

[14] T. Yardibi, J. Li, P. Stoica, M. Xue, and A. B. Baggeroer, "Source localization and sensing: a nonparametric iterative approach based on weighted least squares," *IEEE Trans. Aerospace Electron. Syst.,*, in press.

[15] P. Stoica, J. Li, and J. Ling, "Missing data recovery via a nonparametric iterative adaptive approach," *IEEE Signal Process. Lett.*, vol. 16, no. 4, p. 241244, 2009.

[16] A. Jakobsson, M. Mossberg, M. Rowe, and J. A. S. Smith, "Exploiting Temperature Dependency in the Detection of NQR Signals," *IEEE Transactions on Signal Processing*, vol. 54, no. 5, pp. 1610–1616, May 2006.

[17] P. Stoica, A. Jakobsson, and J. Li, "Cisoid Parameter Estimation in the Colored Noise Case: Asymptotic Cramér-Rao Bound, Maximum Likelihood and Nonlinear Least-Squares," *IEEE Trans. on Signal Processing*, vol. 45, pp. 2048–2059, August 1997.

[18] J. E. Dennis, Jr., *Nonlinear Least Squares*, ser. State of the Art in Numerical Analysis. Academic Press, 1977.

[19] J. J. Moré, *The Levenberg-Marquardt Algorithm: Implementation and Theory*, ser. Numerical Analysis, Lecture Notes in Mathematics 630. Springer Verlag, 1977.

[20] N. Sandgren, Y. Selén, and E. G. Larsson, "Parametric Spectral Analysis of MRS data - on the ambiguity of lineshape modeling," unpublished manuscript.

[21] Y. Yao and S. P. Pandit, "Cramér-Rao Lower Bound for a Damped Sinusoidal Process," *IEEE Trans. Signal Processing*, vol. 43, no. 4, pp. 878–885, April 1995.